Volcanic ash fall events identified using principal component analysis of a high-resolution speleothem trace element dataset

Robert A. Jamieson [a,*], James U.L. Baldini [a], Amy B. Frappier [b,] Wolfgang Müller [c]

[a] Department of Earth Sciences, Durham University, United Kingdom

[b] Department of Geosciences, Skidmore College, NY, United States

[c] Department of Earth Sciences, Royal Holloway University, London, United Kingdom

* Corresponding author at: Department of Earth Sciences, Durham University, United Kingdom. E-mail address: r.a.jamieson@durham.ac.uk

Keywords: stalagmite, principal component analysis, volcanic ash, El Chichón, LA-ICP-MS

Abstract

Large multivariate trace element datasets produced by LA-ICP-MS speleothem analysis can pose difficulties for analysis and interpretation. Processes acting on various timescales and magnitudes affect trace element concentrations, and deconvolving the most important controls is often complex. Here Principal Component Analysis (PCA) is applied to identify the modes and timings of variation which best explain the overall variability in an exceptionally high-resolution (10µm vertical resolution) multivariate trace element record produced by LA-ICP-MS from a modern (1979-2001) Belizean stalagmite with excellent age control.

Principal Component 1 (PC1) in this dataset is defined by a weak correlation between multiple elements, and may reflect non-carbonate material incorporated within the speleothem. Elevated PC1 scores in ATM-7 occur following regional volcanic eruptions with ash clouds extending over the cave site, as demonstrated using NASA remote sensing data from the Total Ozone Mapping Spectrometer and HYSPLIT trajectory modelling. Spikes in PC1 occur at the beginning of the wet season, and this may reflect a seasonal flushing event that transports volcanogenic material through the karst and incorporates it within the speleothem.

Our results suggest that PCA can simplify exploration of large laser ablation datasets, and that PCA is a valuable tool for identifying the dominant controls on stalagmite trace element chemistry. Future studies should evaluate how transferable this technique is to other sites with different environmental conditions where volcanic ashfall has occurred.This research potentially adds tephrochronology to the stalagmite dating toolkit or, conversely, opens the door to using stalagmites to identify previously unknown or uncertainly dated eruptions.

1.1 Introduction

Speleothems are important terrestrial archives of high-resolution palaeoenvironmental information, particularly for low latitudes. They are precisely dateable using a variety of techniques and contain a wealth of different proxy information. Stable isotope ratios are the proxies most commonly used in speleothem research to infer regional climatic information (McDermott, 2004). However, other

proxies including laminae thickness (Baker et al., 2008), optical properties (Proctor et al., 2000), trace element concentrations (Fairchild and Treble, 2009), and calcite density (Zhang et al., 2010) also record various climatic and hydrological information. Trace elements in particular preserve diverse information including both climate (Cruz Jr. et al., 2007) and non-climatic signals such as volcanism (Frisia et al., 2008), land use changes (Borsato et al., 2007) and anthropogenic emissions (Tan et al., 2013).

Detection of volcanic signals in speleothems has focused on two primary avenues of inquiry: indirect records of the effects of volcanism (e.g., aerosol forced cooling (Ridley et al., 2015)) or increased growth rate (Baker et al., 1995)) or direct evidence of volcanism (e.g., elevated sulphate concentrations in speleothems; (Frisia et al., 2005)). The former is generally inferred based on stable isotope ratios (Ridley et al., 2015) as hydrological or temperature records, whilst direct detection of volcanogenic material has thus far focused on measuring extremely low trace element concentrations using techniques such as synchrotron radiation based micro X-ray fluorescence (Frisia et al., 2005; Frisia et al., 2008). Higher detection limits and an inability to measure certain elements due to common polyatomic interferences (such as high counts of $^{16}O_2$ swamping any ^{32}S signal (Reed et al., 1994)) complicate the detection of volcanogenic material using more widely available techniques such as inductively coupled plasma mass spectrometry (ICP-MS). However, these limitations can be overcome by examining multivariate ICP-MS data using methods that examine the covariation of multiple elements derived from volcanogenic sources.

Here we use Principal Component Analysis (PCA) of high-resolution LA-ICP-MS data to detect the signal of volcanic ash deposition in a Belizean stalagmite. PCA is a multivariate statistical analysis technique used to identify the modes of variation within a multivariate dataset which best explain the overall variability (Abdi and Williams, 2010). For example, PCA has been successfully applied to identify distinct signatures of components carried in separate air masses (e.g. atmospheric dust versus sea ice aerosols) from a multivariate dataset of elemental measurements of ice cores, and principal component scores plotted as a time series produced a record of the significance of different components over time (Mayewski et al., 1994). In a speleothem context, this technique could identify different modes of trace element variation within a time series. This method allows the deconvolution of signals such as volcanism from the background variation in a multivariate trace element dataset.

2.1 Methods

Stalagmite ATM7 was collected in January 2001 from Actun Tunichil Muknal (ATM) in central Belize (Figure 1), dated using radiometric (^{137}Cs) and layer-counting methods (Frappier et al., 2002), and $\delta^{13}C$ and $\delta^{18}O$ records produced and published (Frappier et al., 2002; Frappier et al., 2007). Frappier et al. (2002) interpreted $\delta^{13}C$ variability as a proxy for ENSO driven changes in the soil and local ecosystem carbon cycle. Frappier et al. (2007) interprets $\delta^{18}O$ variability as a proxy for rainfall amount, including a record of short-lived negative spikes in $\delta^{18}O$ during tropical cyclone events.

Trace element concentrations were measured using a prototype RESOlution M-50 excimer (193 nm) laser-ablation system with two-volume laser-ablation cell coupled to an Agilent 7500ce/cs

quadrupole ICPMS at Royal Holloway University, London. Full description of the analytical setup, as well as initial performance metrics can be found in Müller et al. (2009).

Eleven ablation tracks were measured using a 140 by 10µm rectangular laser slit across sections of ATM7 (Figure 2) such that the entire length of the stalagmite was measured by at least three parallel tracks. Prior to measurement, all tracks were pre-ablated to remove any superficial contamination. A 15Hz repetition rate of a 90mJ laser spot and a stage scan speed of 10µm s^{-1} were used during the main track measurement. Two stalagmite areas were ablated for elemental mapping using a circular spot size of 34µm along tracks 50µm apart at a scan speed of 50µm s^{-1}. Speleothem analyses were bracketed by analyses of NIST 612, NIST 610 and MACS3 standards for quantification.

Data reduction was performed using the Iolite software package using NIST 610/612 standards for external standardisation (Paton et al., 2011). Calcium-43 was measured throughout the sample runs as an internal standard.

Individual ablation tracks were aligned using a "wiggle-matching" tuning technique to align variation in magnesium concentrations onto a single absolute distance scale shared between all tracks. This method allowed the combination of these datasets whilst also taking into account minor lateral variation in lamina thickness. The lateral consistency in magnesium concentrations in the mapped areas shows this approach to be a viable method to combine transects (Figure 3). All data were then linearly interpolated to allow averaging between the eleven different tracks at the same distance/time intervals. Values at each distance interval outside two standard deviations of the mean were excluded from the final averaged values to remove any outliers, which may have resulted from contamination or heterogeneous areas of the stalagmite. The absolute distance scale was then converted to the age model of Frappier et al., 2007 by matching the final magnesium record to their $\delta^{13}C$ record. Good topological agreement between the Mg and $\delta^{13}C$ time-series data, both proxies for rainfall at this tropical site, strongly support this approach. Comparison of distance versus age between the stable isotope measurements and the laser ablation tracks show good similarity, with some slight variations resulting from varying growth rates laterally between the micromilled isotope track and the ablation tracks.

To process the trace element dataset prior to performing PCA the data were normalized by calculating the z-scores of each dataset to eliminate PCA's sensitivity to the scaling of the variables. The principal component coefficients, component scores, and percentage variance explained were calculated using the *pca* function in MATLAB (MathWorks, 2013).

Time periods where volcanic ash clouds were present over the cave site were identified using satellite maps of aerosol distributions obtained from the NASA Total Ozone Mapping Spectrometer (TOMS) Volcanic Image Archive for eruptions for which these maps were available. Earth Probe (TOMSEPL3.008) and Nimbus-7 (TOMSN7L3.008) version 8 TOMS daily level 3 global 1.0°x1.25° gridded Aerosol Index data provide a qualitative UV absorbing aerosol record over central and northern Belize (Acker and Leptoukh, 2007; Carn et al., 2003; Krueger et al., 2008).

The NOAA Air Resources Laboratory HYSPLIT Volcanic Ash model was used to compute ash cloud trajectories for eruptions to confirm the aerosol data and increase confidence that the ash cloud had in fact reached the cave site (Draxler and Rolph, 2003; Rolph, 2003). Volcanic Explosivity Index values for known eruptions were used to estimate approximate plume heights (Newhall and Self, 1982).

3.1 Results and Discussion

3.1.1 Principal Component 1

Principal component analysis of the 20-element trace element dataset generated for ATM7 yields a first principal component which explains 81.9% of the variability within the dataset. Principal Component 1 (PC1) consists of a weak correlation between all of the analysed elements, many of which are typically excluded from calcite (Table 1), and probably represents non-calcite material incorporated in the speleothem. The PC1 score time series is characterised by short period high amplitude spikes indicating that, although it explains a substantial portion of the variation within the dataset, PC1 is only a dominant control during infrequent short-lived events (Figure 4).

Previous studies have documented peaks in elements such as Zn, Cu, Pb, Y and other metals as a pulse of colloidally transported material driven by a seasonal flushing event (Borsato et al., 2007; Hartland et al., 2012). In this dataset these signals do not occur annually, but instead occur sporadically through the record. Notably however, in years when they do occur, the spikes are synchronous with the wet season onset as inferred from Mg concentrations (Figure 6) where a flushing event would typically occur.

We suggest that the observed signal is in fact recording a seasonal flushing event at our site; however, this event is evident only after sufficient raw material has been delivered to the karst to generate detectable levels of these elements. Tropical karst soils are depleted in many micronutrients due to high levels of biological productivity as well as leaching from high rainfall (Vitousek and Sanford, 1986). Substantial additional trace elements delivered to the ATM cave system are limited to particulate material sourced from wind-blown dust or volcanic ash, as the only sources of material above the cave are the karst, thin soil and canopy forest.

The NASA TOMS Aerosol Index dataset identifies intervals when aerosol levels are elevated in the atmosphere over the ATM cave site. Three primary sources of aerosols contribute to elevated Aerosol Index values over central and northern Belize: i) a seasonal signal of wood ash derived from biomass burning (Prins et al., 2003), ii) short-lived spikes in El Niño years corresponding to increased wildfires (Peppler et al., 2000), and iii) volcanic ash plumes over the area (Krueger et al., 2008). Correlation with records of known eruptions in Central America and the Caribbean (Smithsonian, 2014) (Figure 4) as well as HYSPLIT trajectory modelling of those eruptions (Figure 5) allows identification of intervals of elevated Aerosol Index where volcanic ash is transported over the cave site. Significant spikes in PC1 scores occur at the onset of the wet season following volcanic eruptions that produced an identifiable increase in the TOMS Aerosol Index over the cave site (Figures 4 and 7). These spikes record the addition and subsequent flushing of material by volcanic ashfall from these eruptions. Aerosol spikes not corresponding to historical eruptions probably reflect biomass burning which produces aerosols composed primarily of carbon and therefore do not have a subsequent spike in PC1 score.

A comparison of seasonal trace element variability for all years with (Figure 7a) and without (Figure 7b) eruptions recorded in the stalagmite record clearly demonstrates the difference resulting from the addition of volcanogenic material to the dripwater. In both cases, magnesium concentrations are

used to infer seasonality. Mg concentrations gradually rise through the dry season as mean dripwater residence time in the karst increases, then decreases precipitously to a lower baseline level through the wet season. This pattern is consistent through years with and without eruptions. A slight uptick in concentrations occurs in August and September, particularly years with eruptions, which may record the "little dry" midsummer drought which occurs in the region (Magaña et al., 1999).

Lead spikes occur at the onset of the wet season in most years, however in years without eruptions the spikes are barely above the mean background levels at only 1-2ppm. During wet season deposition following volcanic eruptions significant spikes of up to 15ppm of lead occur. This is apparent even in the normalised data, where the post-eruption spike is significantly above the background level of the rest of the year. These spikes coincide with, and indeed are part of, spikes in PC1 scores.

The temporal offset between the eruption date and the recorded spike in the stalagmite record varies from year to year. This reflects eruptions occurring at differing times of the year, rather than the timing of the spike changing. The eruption is always recorded at the start of the wet season following the eruption; this can lead to lags of from between two months up to one year (Figure 8). This is true of eruptions occurring in either the dry and wet seasons, as volcanogenic material appears to remain in the soil or karst until flushed through at the start of the subsequent wet season. A possible explanation for this phenomenon is the fact that particle and colloid release from soil is at its highest during the initial irrigation of the soil (El-Farhan et al., 2000). Flushes of volcanogenic material may only occur when both the material itself and sufficient mobile organic matter is present to transport it. Additionally, some studies have suggested that the mobilisation of elements such as lead are linked to the magnitude of rainfall events (Jo et al., 2010). Hartland et al. (2012) suggest that in regions with large seasonal extremes the kinetic energy of flow may be important to the transport of particulate organic matter and associated elements. Each of these factors would lead to volcanic ash deposition only being recorded in the stalagmite during the first large initial rainfall event of the wet season following the eruption.

3.2 Recorded Eruptions

3.2.1 El Chichón (Mexico)

The very large VEI 5 April 1982 eruptions of El Chichón erupted approximately 0.38km^3 direct rock equivalent (DRE) of juvenile material and 0.16km^3 DRE of lithic material, much of which erupted in a 17km high ash cloud which extended across a large area of Central America (Rose and Durant, 2008; Varekamp et al., 1984). TOMS aerosol data (Figure 5) demonstrates that an ash cloud extended over Central and northern Belize. Earlier trace element work on ATM-7 using Empirical Orthogonal Function analysis (Frappier, 2006) identified a major perturbation in dripwater chemistry in 1982 that was attributed to the El Chichón eruption. This analysis reproduces that signal using new higher-resolution trace element data whilst also identifying several other comparable events from the rest of the time series.

3.2.2 Concepción (Nicaragua)

A VEI 2 Concepción eruption (March 1983) also produced a detectable spike in aerosol levels over Belize. This is followed by a small amplitude spike in PC1. The reduced size of this spike may be the result of a smaller amount of ash delivered to the cave site from this eruption resulting in a weaker signal. Meteorological conditions at the time produced a more diffuse ash cloud which HYSPLIT modelling suggests was carried eastwards over the Caribbean Sea (Figure 5). The modelled ash distribution does not show the ash cloud passing over the cave directly, but the small spike in TOMS aerosol data at the time may suggest that some of the ash was deposited over the cave site.

3.2.3 Arenal (Costa Rica)

Arenal has been erupting intermittently since 1968 and experienced a significant period of column collapses and pyroclastic flows in 1987-1989 (Cole et al., 2005). These eruptive events are not apparent as large elevations of TOMS aerosol levels, but could conceivably deliver material to the cave site over a sustained period resulting in the low amplitude, longer period signal observed in the PC1 time series. The lack of corroborating TOMS evidence for an ash cloud from Arenal coincident with this signal means that we have low confidence that this eruption is truly recorded. HYSPLIT modelling of one of the larger eruptions of Arenal during this time period shows the ash cloud being carried westwards (Figure 5), but this does not preclude the possibility of one of the many smaller eruptive episodes resulting in an ash cloud reaching the cave site at another time. In summary, Arenal can be neither confirmed nor ruled out as the source of this PC1 spike, but remains the most probable source.

3.2.4 Colima (Mexico) and Pinatubo (Phillipines)

The VEI 2 eruption of Colima in early 1991 is the most distant eruption that apparently influenced the geochemistry of the ATM7 stalagmite. It is recorded largely because of fortuitous wind conditions following the eruption. HYSPLIT modelling illustrates that the ash cloud passed directly over central Belize (Figure 5), very strongly suggesting that Colima is the source of elevated aerosol levels and the initial PC1 signal in 1991. However, the double spike in PC1 is somewhat difficult to explain based on a single eruptive event. This signal suggests either a short period of time when transport of ash sourced elements to the karst stopped prior to a second flush, or a second source of material.

The June 1991 Mount Pinatubo eruption (VEI 6) was the largest volcanic eruption of the late 20th Century (Newhall and Punongbayan, 1996; Torres et al., 1995), erupting 1.8-2.2km^3 DRE of tephra as a 40km high column (Wiesner et al., 2003). Although no clear signal of the eruption exists in the TOMS data over Belize it is conceivable that some material from the eruption was capable of reaching the cave site in the months subsequent to the eruption. Mount Pinatubo and Actun Tunichil Muknal are at similar latitudes, of 15 degrees and 17 degrees respectively, and aerosols (although not necessarily ash) from the eruption were detectable in the atmosphere above the Caribbean for over a year after the eruption (Antuña, 1996). Any ash transported this distance would have been diffuse in both concentration and timing so therefore may not have registered above the background summer signal of biomass burning over Belize but could have accumulated in the soil over time. The available data cannot differentiate between Pinatubo or a second flush of remaining material from Colima as the cause of the second PC1 spike.

3.2.5 Rincón de la Vieja (Costa Rica)

The February 1998 Rincón de la Vieja eruption (VEI 2), is apparent as a large aerosol spike over the cave site. This is subsequently followed by a large, short-lived spike in PC1 scores at the onset of the subsequent wet season. HYSPLIT modelling demonstrates that the ash cloud from this eruption was carried northwards over the Caribbean Sea over the first 48 hours following the eruption, from where the prevailing easterlies would carry the ash over the cave site (Figure 5).

3.2.6 Fuego (Guatemala)

Volcán de Fuego in Guatemala began a period of increased activity in May 1999 with a VEI 2 eruption (Lyons et al., 2009). This eruption produced a small but detectable increase in aerosol levels and is subsequently followed by a spike in PC1 scores. HYSPLIT modelling confirms that a significant portion of the ash cloud was blown eastwards towards ATM (Figure 5).

3.3 Unrecorded Eruptions and Potential False Positives

Not all eruptions in Central America during the depositional period are apparent in the ATM-7 trace element record (Figure 4). This is clearly attributable to ash only reaching the cave site when wind and ash plume conditions are in the correct configuration. Because prevailing winds in this region are the easterly trade winds (Polzin et al., 2014) this results in the majority of ash clouds being carried away from the cave and over the Pacific Ocean. Eruptions are only recorded when the wind conditions at the time of eruption are such that ash clouds are carried eastwards over the cave site. HYSPLIT modelling for several recorded eruptions demonstrate that wind fields at the time of the recorded eruptions do indeed carry ash clouds over the cave site (Figure 5 – a-b,d-f). Whilst HYSPLIT modelling of an unrecorded or uncertain eruption do not show an ash cloud over the cave site (Arenal – Figure 5c).

Several small magnitude spikes in PC1 score occur throughout the record which we have not linked to known eruptions. The spike in 1979 corresponds to a prominent red layer visible in the stalagmite (Figure 3), that was deposited during a year of extreme rainfall where precipitation in the area was almost three standard deviations above the mean (reflected by low stable oxygen and carbon isotope values within the same layer). We suggest that this spike occurs due to an area of high levels of detrital material and low density calcite. The lower proportion of calcite in this section of the stalagmite would result in the data reduction procedure applied here overestimating the trace element content. As such, we believe that this spike probably results from extremely atypical weather, rather than a volcanic signal.

The remaining small spikes in late 1981, late 1988/early 1989 and 1995 are very low in amplitude (<0.5), suggesting that the PC1 relationship between variables is much weaker during these events. Indeed, they are at or below background in several of the trace elements measured (e.g. Fe, Rb, Cd, Si and potentially Th – see figures S1-S4). These spikes are not associated with elevated aerosol levels above the cave or known volcanic eruptions, but may result from the diffuse delivery of material, flushing of residual material within the soil or another unknown source that we are unable to identify from the available data.

3.4 Geochemistry of Eruptions

Examining the elemental concentrations at the stalagmite depths corresponding to the spikes in PC1 (Figure 9) enables comparison of the chemistry of each presumed volcanic ash signal. Elemental

concentrations were normalised by ratioing to lead to eliminate differences due to varying amounts of ash incorporation, assuming that the majority of lead incorporated within the speleothem is solely from a volcanic source. These values were also compared to the mean value of calcite with the lowest PC1 scores (n=100) to provide a non-volcanic baseline to compare against. A sample of El Chichón ash obtained from the Smithsonian Institution was analysed by solution ICP-MS to assess the potential for fingerprinting specific eruptions.

Each ash influenced depth interval is broadly similar in elemental profile with similar values of each elemental ratio relative to the other elements measured. This is consistent with broadly similar material (i.e. volcanic ash) being present in each one. Of particular note is the much higher Al/Pb relative to the other elements. In the low PC1 value calcite the Al/Pb ratio is similar to the Ba/Pb and Sr/Pb ratios, whilst in the ash influenced series and ash sample itself the Al/Pb ratio is approximately two orders of magnitude higher. This may suggest the incorporation of aluminosilicate material into the speleothem. This is consistent with the incorporation of clay or feldspar minerals, both common constituents of volcanic ash.

The El Chichón ash sample cannot be definitively matched to the El Chichón PC1 spike rather than the other spikes based on geochemistry alone. This suggests that biogeochemical processing of volcanogenic material in the soil and karst complicates geochemical fingerprinting of eruption- or volcano-specific ash in a speleothem. Several processes between source and sink alter the elemental distributions of the analysed elements. Cycling in the soil and nutrient uptake by overlying vegetation will preferentially lower the concentrations of certain elements. Elements will respond differently to adsorption and chemical reactions in the soil, as well as being flushed though the karst preferentially as a result of binding to different organic matter fractions (Hartland et al., 2012). For example, lead and yttrium have a much greater binding affinity to soil organic matter than most other measured metals (Baldini et al., 2012; Hartland et al., 2012). Future studies focusing on elements that behave similarly between deposition and incorporation may prove more effective. A possible candidate for such a study would be the rare earth elements, although REE measurement challenging by very low concentrations within speleothems and natural waters (Aliaga-Campuzano et al., 2013).

4.1 Implications and Future Work

Principal component analysis of high-resolution trace element datasets has the potential to produce speleothem eruption records that complement and supplement ice core and sediment tephrochronology, providing a precisely dated, low-latitude, continental, and regional archive of ash deposition even after removal or reworking of surface sediments. Eruptions recorded in ice cores that influence global climate, but which are of unknown location, could be more accurately located to within a specific region using this technique. Additionally, the high precision of speleothem dating allows determination of precise dates of eruptions (such as the Minoan eruption of Santorini), which are disputed or imprecisely dated by archaeological, stratigraphic or historical records (Friedrich et al., 2006). Geological records of prehistoric records are exceptionally incomplete, with estimates for the percentage of known events less than 0.17% globally for eruptions 5-20Ka and as low as 0.0005% for some regions (Watt et al., 2013). This technique enables the use of speleothems as an additional archive of eruption records, particularly in tropical areas where historical eruption records are often

poor. Improved eruption records allow better estimation of recurrence intervals and are essential for assessing volcanic hazards.

In this study remote sensing and meteorological data very strongly suggest that PC1 reflected volcanic ash deposition by linking PC1 spikes to specific historical eruptions. Studies extending further into the past (e.g., beyond the satellite or historical record) will not have this information available. However, these studies could still apply this technique by first calibrating a PC record using modern information, and then extend interpretations back through time. Similar PC spikes as those reflecting historical volcanic ash deposition are interpretable as unknown volcanic eruptions. Furthermore, a modern calibration provides information regarding the proportion of regional eruptions detectable at a specific cave site, as well as any false positives. The proof-of-concept study presented here captured 5 out of 5 volcanic eruptions that produced aerosol clouds that passed over the cave site, and 5 out of 28 total Central American eruptions larger than VEI 2. Studies of older stalagmites that were not growing during historical times could still benefit from the technique, but determination of the stalagmite's sensitivity to eruptions would remain unknown.

Speleothem trace element eruption records can also function as chronological markers. The date of a well-recorded eruption detected in a speleothem can be incorporated into the age model, providing even greater precision in speleothem dating.

Additional future work could focus on further confirming that the trace element spikes recorded in this stalagmite by PC1 are indeed the results of volcanic ash deposition. Geochemical techniques which are impractical for analysis of an entire stalagmite could be employed now that the physical location of the spike within the sample is known. These include employing sulphur isotopes (Frisia et al., 2005; Frisia et al., 2008) or using synchrotron radiation based micro X-ray fluorescence to detect elements diagnostic of volcanism which are only present in low concentrations such as Br or Mo (Badertscher et al., 2014).

4.2 Comparison to Previous Work

These trace element results are consistent with previous work which suggested that the El Chichón eruption was recorded in the trace elements of ATM-7 (Frappier, 2006), as well as detecting several additional volcanic ash deposition events to the record. Magnesium concentrations are broadly similar to $\delta^{13}C$, showing similar patterns in response to seasonality and El Nino events as in Frappier et al. (2002). Trace elements do not show a clear response to the tropical cyclone events which are observed in the $\delta^{18}O$ record (Frappier et al., 2007). We suggest that although tropical cyclone rainfall is isotopically distinct from normal rainfall it does not represent a substantial additional volume, and therefore has a much smaller influence on trace element proxies for precipitation.

5.1 Conclusions

Here we show the potential of Principal Component Analysis as a statistical technique for exploratory analysis of large stalagmite trace element datasets. The technique can deconvolve the different modes of trace element variation and, when principal components are linked to physical processes or inputs, can produce time series of the shifting influence of those modes of variation. For a stalagmite where intermittent signals such as the addition of volcanic ash material are recorded, this technique can clearly identify these discrete events within the record. It is important

to note that Principal Component Analysis of individual trace element datasets will produce unique principal components and correlation coefficients. Volcanic ash deposition may not always appear as the first principal component; instead, it may explain a lower proportion of the variability or consist of slightly different elemental distributions due to local soil or plant chemistry. However, for any stalagmite where volcanic ash deposition has a measurable influence on stalagmite geochemistry PCA should produce a corresponding principal component.

We demonstrate that the stalagmite ATM-7 from Actun Tunichil Muknal cave in central Belize records the occurrence of volcanic ash deposition over the cave site. Comparison of ashfall events recorded in speleothems can be used as a tephrochronological tool in conjunction with existing local historical, archaeological or sedimentological records. Additionally, analysis of stalagmites using this technique can yield absolutely dated, high resolution, low latitude records of volcanic eruptions, providing important low latitude counterparts to volcanogenic sulphate records in glacial ice cores.

Acknowledgements

TOMS Time Series analyses used in this study were produced with the Giovanni online data system, developed and maintained by the NASA GES DISC. The authors gratefully acknowledge the NOAA Air Resources Laboratory (ARL) for the provision of the HYSPLIT transport and dispersion model and READY website (http://www.arl.noaa.gov/ready.php) used in this publication. Eruption timings and magnitudes sourced from the Smithsonian Institution Global Volcanism Program unless otherwise specified.

The Division of Petrology and Volcanology, Department of Mineral Sciences, Smithsonian Institution kindly provided El Chichón ash sample NMNH 115695 to A. Frappier.

This research was supported the European Research Council (240167).

We gratefully thank our three anonymous reviewers for their useful comments and critique of the manuscript.

References

Abdi, H., Williams, L.J., 2010. Principal component analysis. Wiley Interdisciplinary Reviews: Computational Statistics 2, 433-459.

Acker, J.G., Leptoukh, G., 2007. Online Analysis Enhances Use of NASA Earth Science Data. EOS, Transactions, American Geophysical Union 88, 14-17.

Aliaga-Campuzano, M.P., Bernal, J.P., Briceno-Prieto, S.B., Perez-Arvizu, O., Lounejeva, E., 2013. Direct analysis of lanthanides by ICPMS in calcium-rich water samples using a modular high-efficiency sample introduction system-membrane desolvator. Journal of Analytical Atomic Spectrometry 28, 1102-1109.

Antuña, J.C., 1996. Lidar measurements of stratospheric aerosols from Mount Pinatubo at Camaguey, Cuba. Atmospheric Environment 30, 1857-1860.

Badertscher, S., Borsato, A., Frisia, S., Cheng, H., Edwards, R.L., Tüysüz, O., Fleitmann, D., 2014. Speleothems as sensitive recorders of volcanic eruptions – the Bronze Age Minoan eruption recorded in a stalagmite from Turkey. Earth and Planetary Science Letters 392, 58-66.

Baker, A., Smart, P.L., Barnes, W.L., Edwards, R.L., Farrant, A., 1995. The Hekla 3 volcanic eruption recorded in a Scottish speleothem? The Holocene 5, 336-342.

Baker, A., Smith, C.L., Jex, C.N., Fairchild, I.J., Genty, D., Fuller, L., 2008. Annually Laminated Speleothems: a Review. International Journal of Speleology 37, 193-206.

Baldini, J.U.L., McDermott, F., Baldini, L.M., Ottley, C.J., Linge, K.L., Clipson, N., Jarvis, K.E., 2012. Identifying short-term and seasonal trends in cave drip water trace element concentrations based on a daily-scale automatically collected drip water dataset. Chemical Geology.
Borsato, A., Frisia, S., Fairchild, I.J., Somogyi, A., Susini, J., 2007. Trace element distribution in annual stalagmite laminae mapped by micrometer-resolution X-ray fluorescence: implications for incorporation of environmentally significant species. Geochimica et Cosmochimica Acta 71, 1494-1512.
Carn, S.A., Krueger, A.J., Bluth, G.J.S., Schaefer, S.J., Krotkov, N.A., Watson, I.M., Datta, S., 2003. Volcanic eruption detection by the Total Ozone Mapping Spectrometer (TOMS) instruments: a 22-year record of sulphur dioxide and ash emissions. Geological Society, London, Special Publications 213, 177-202.
Cole, P.D., Fernandez, E., Duarte, E., Duncan, A.M., 2005. Explosive activity and generation mechanisms of pyroclastic flows at Arenal volcano, Costa Rica between 1987 and 2001. Bulletin of Volcanology 67, 695-716.
Cruz Jr., F.W., Burns, S.J., Jercinovic, M., Karmann, I., Sharp, W.D., Vuille, M., 2007. Evidence of rainfall variations in Southern Brazil from trace element ratios (Mg/Ca and Sr/Ca) in a Late Pleistocene stalagmite. Geochimica et Cosmochimica Acta 71, 2250-2263.
Draxler, R.R., Rolph, G.D., 2003. HYSPLIT (HYbrid Single-Particle Lagrangian Integrated Trajectory) Model NOAA Air Resources Laboratory, Silver Spring, MD.
El-Farhan, Y.H., Denovio, N.M., Herman, J.S., Hornberger, G.M., 2000. Mobilization and Transport of Soil Particles during Infiltration Experiments in an Agricultural Field, Shenandoah Valley, Virginia. Environmental Science and Technology 34, 3555-3559.
Fairchild, I.J., Treble, P.C., 2009. Trace elements in speleothems as recorders of environmental change. Quaternary Science Reviews 28, 449-468.
Frappier, A., Sahagian, D., Gonzalez, L.A., Carpenter, S.J., 2002. El Nino events recorded by stalagmite carbon isotopes. Science 298, 565-565.
Frappier, A.B., 2006. Empirical orthogonal function analysis of multivariate stalagmite trace element data: Detecting the 1982 El Chichón volcanic eruption. Archives of Climate Change in Karst, Karst Waters Institute Special Publication 10, 113-115.
Frappier, A.B., Sahagian, D., Carpenter, S.J., González, L.A., Frappier, B.R., 2007. Stalagmite stable isotope record of recent tropical cyclone events. Geology 35, 111.
Friedrich, W.L., Kromer, B., Friedrich, M., Heinemeier, J., Pfeiffer, T., Talamo, S., 2006. Santorini Eruption Radiocarbon Dated to 1627–1600 B.C. Science 312, 548.
Frisia, S., Borsato, A., Fairchild, I.J., Susini, J., 2005. Variations in atmospheric sulphate recorded in stalagmites by synchrotron micro-XRF and XANES analyses. Earth and Planetary Science Letters 235, 729-740.
Frisia, S., Borsato, A., Susini, J., 2008. Synchrotron radiation applications to past volcanism archived in speleothems: An overview. Journal of Volcanology and Geothermal Research 177, 96-100.
Hartland, A., Fairchild, I.J., Lead, J.R., Borsato, A., Baker, A., Frisia, S., Baalousha, M., 2012. From soil to cave: Transport of trace metals by natural organic matter in karst dripwaters. Chemical Geology 304-305, 68-82.
Jo, K.-n., Woo, K.S., Hong, G.H., Kim, S.H., Suk, B.C., 2010. Rainfall and hydrological controls on speleothem geochemistry during climatic events (droughts and typhoons): An example from Seopdong Cave, Republic of Korea. Earth and Planetary Science Letters 295, 441-450.
Krueger, A., Krotkov, N., Carn, S., 2008. El Chichon: The genesis of volcanic sulfur dioxide monitoring from space. Journal of Volcanology and Geothermal Research 175, 408-414.
Lyons, J.J., Waite, G.P., Rose, W.I., Chigna, G., 2009. Patterns in open vent, strombolian behavior at Fuego volcano, Guatemala, 2005–2007. Bulletin of Volcanology 72, 1-15.
Magaña, V., Amador, J.A., Medina, S., 1999. The Midsummer Drought over Mexico and Central America. Journal of Climate 12, 1577-1588.

MathWorks, 2013. MATLAB and Statistics Toolbox Release 2013a. The MathWorks Inc., Natick, Massachusetts, United States.
Mayewski, P.A., Meeker, L.D., Whitlow, S., Twickler, M.S., Morrison, M.C., Bloomfield, P., Bond, G.C., Alley, R.B., Gow, A.J., Meese, D.A., Grootes, P.M., Ram, M., Taylor, K.C., Wumkes, W., 1994. Changes in Atmospheric Circulation and Ocean Ice Cover over the North Atlantic During the Last 41,000 Years. Science 263, 1747-1751.
McDermott, F., 2004. Palaeo-climate reconstruction from stable isotope variations in speleothems: a review. Quaternary Science Reviews 23, 901-918.
Medina-Elizalde, M., Rohling, E.J., 2012. Collapse of Classic Maya civilization related to modest reduction in precipitation. Science 335, 956-959.
Müller, W., Shelley, M., Miller, P., Broude, S., 2009. Initial performance metrics of a new custom-designed ArF excimer LA-ICPMS system coupled to a two-volume laser-ablation cell. Journal of Analytical Atomic Spectrometry 24, 209.
Newhall, C.G., Punongbayan, A.S., 1996. Fire and Mud: Eruptions and Lahars of Mount Pinatubo, Philippines. University of Washington Press, Seattle.
Newhall, C.G., Self, S., 1982. The Volcanic Explosivity Index (VEI): An estimate of explosive magnitude for historical volcanism. Journal of Geophysical Research 87, 1231-1238.
Paton, C., Hellstrom, J., Paul, B., Woodhead, J., Hergt, J., 2011. Iolite: Freeware for the visualisation and processing of mass spectrometric data. Journal of Analytical Atomic Spectrometry 26, 2508.
Peppler, R.A., Bahrmann, C.P., Barnard, J.C., Campbell, J.R., Cheng, M.-D., Ferrare, R.A., Halthore, R.N., Heilman, L.A., Hlavka, D.L., Laulainen, N.S., Lin, C.-J., Ogren, J.A., Poellot, M.R., Remer, L.A., Sassen, K., Spinhirne, J.D., Splitt, M.E., Turner, D.D., 2000. ARM Southern Great Plains Site Observations of the Smoke Pall Associated with the 1998 Central American Fires. Bulletin of the American Meteorological Society 81, 2563-2591.
Polzin, D., Guirola, L.G., Hastenrath, S., 2014. Climatic variations in Central America: further exploration. International Journal of Climatology, n/a-n/a.
Prins, E.M., Schmidt, C.C., Feltz, J.M., Reid, J.S., Westphal, D.L., Richardson, K., 2003. A two-year analysis of fire activity in the western hemisphere as observed with the GOES wildfire automated biomass burning algorithm. American Meteorological Society Paper P2.28. Reprint #3298.
Proctor, C.J., Baker, A., Barnes, W.L., Gilmour, R.A., 2000. A thousand year speleothem proxy record of North Atlantic climate from Scotland. Climate Dynamics 16, 815-820.
Reed, N.M., Cairns, R.O., Hutton, R.C., Takaku, Y., 1994. Characterization of polyatomic ion interferences in inductively coupled plasma mass spectrometry using a high resolution mass spectrometer. Journal of Analytical Atomic Spectrometry 9, 881.
Ridley, H.E., Asmerom, Y., Baldini, J.U.L., Breitenbach, S.F.M., Aquino, V.V., Prufer, K.M., Culleton, B.J., Polyak, V., Lechleitner, F.A., Kennett, D.J., Zhang, M., Marwan, N., Macpherson, C.G., Baldini, L.M., Xiao, T., Peterkin, J.L., Awe, J., Haug, G.H., 2015. Aerosol forcing of the position of the intertropical convergence zone since AD 1550. Nature Geoscience.
Rolph, G.D., 2003. Real-time Environmental Applications and Display sYstem (READY) Website. NOAA Air Resources Laboratory, Silver Spring, MD. .
Rose, W.I., Durant, A.J., 2008. El Chichón volcano, April 4, 1982: volcanic cloud history and fine ash fallout. Natural Hazards 51, 363-374.
Smithsonian, 2014. Global Volcanism Program. Smithsonian Institution, http://volcano.si.edu/.
Tan, L., Shen, C.-C., Cai, Y., Lo, L., Cheng, H., An, Z., 2013. Trace-element variations in an annually layered stalagmite as recorders of climatic changes and anthropogenic pollution in Central China. Quaternary Research.
Torres, O., Herman, J.R., Bhartia, P.K., Ahmad, Z., 1995. Properties of Mount Pinatubo aerosols as derived from Nimbus 7 total ozone mapping spectrometer measurements. Journal of Geophysical Research 100, 14043-14045.

500 Varekamp, J.C., Luhr, J.F., Prestegaard, K.L., 1984. The 1982 eruptions of El Chichón Volcano
501 (Chiapas, Mexico): Character of the eruptions, ash-fall deposits, and gasphase. Journal of
502 Volcanology and Geothermal Research 23, 39-68.
503 Vitousek, P.M., Sanford, R.L., 1986. Nutrient Cycling in Moist Tropical Forest. Annu Rev Ecol Syst 17,
504 137-167.
505 Watt, S.F.L., Pyle, D.M., Mather, T.A., 2013. The volcanic response to deglaciation: Evidence from
506 glaciated arcs and a reassessment of global eruption records. Earth-Science Reviews 122, 77-102.
507 Wiesner, M.G., Wetzel, A., Catane, S.G., Listanco, E.L., Mirabueno, H.T., 2003. Grain size, areal
508 thickness distribution and controls on sedimentation of the 1991 Mount Pinatubo tephra layer in the
509 South China Sea. Bulletin of Volcanology 66, 226-242.
510 Zhang, D., Zhang, P., Sang, W., Cheng, H., Wu, X., Yuan, Y., Bai, Y., Wang, J., Jia, J., 2010. Implications
511 of stalagmite density for past climate change: An example from stalagmite growth during the last
512 deglaciation from Wanxiang Cave, western Loess Plateau. Chinese Science Bulletin 55, 3936-3943.

513

514

Figure List

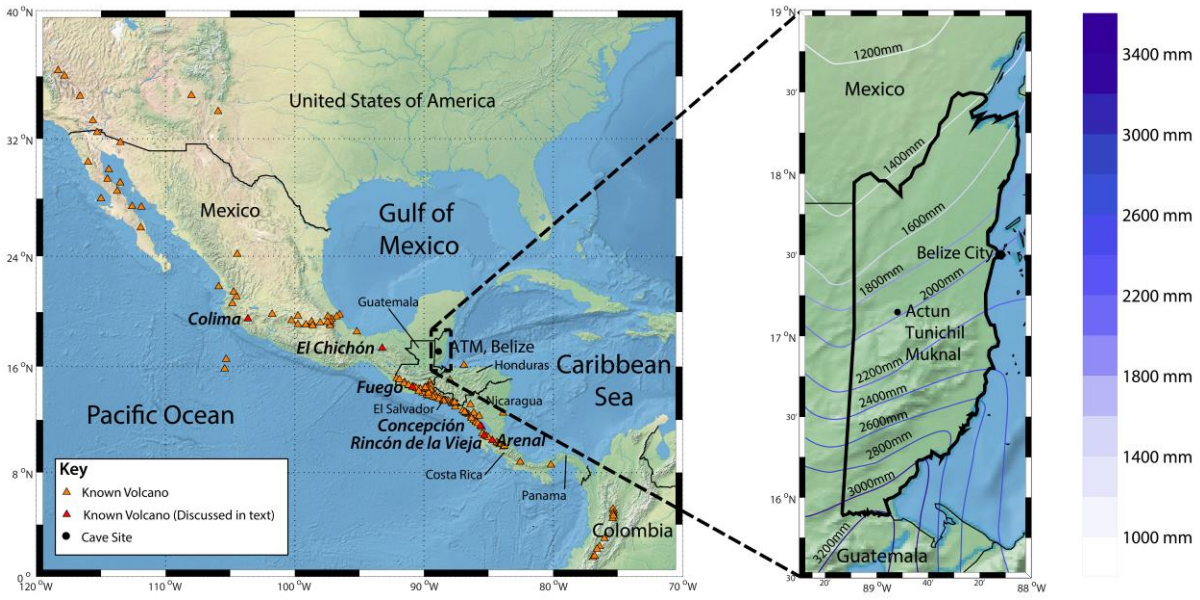

Figure 1: Left: Location of Actun Tunichil Muknal and all volcanoes in Central America. Right: Location of ATM in Belize, with contoured mean annual rainfall (Medina-Elizalde and Rohling, 2012).

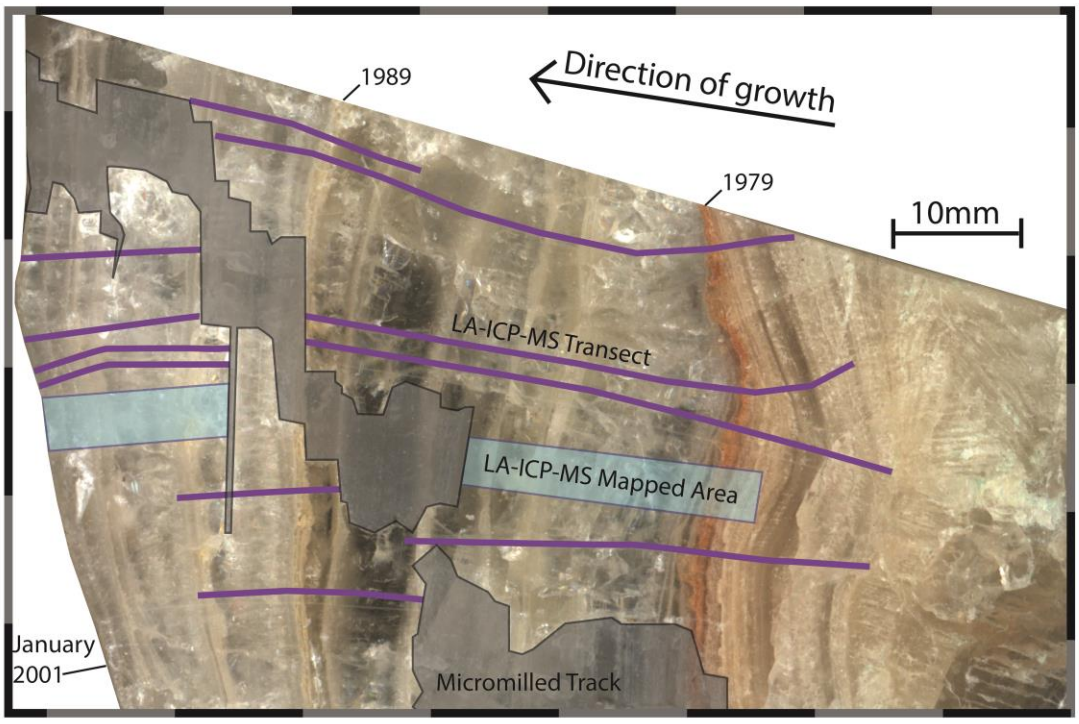

Figure 2: Polished section of ATM7 used in this study. Black outlines with grey shading highlight micromilled track used for generating the stable isotope records used in Frappier et al. (2002) and Frappier et al. (2007). Purple lines show laser ablation tracks. Blue shaded areas show areas of laser ablation mapping.

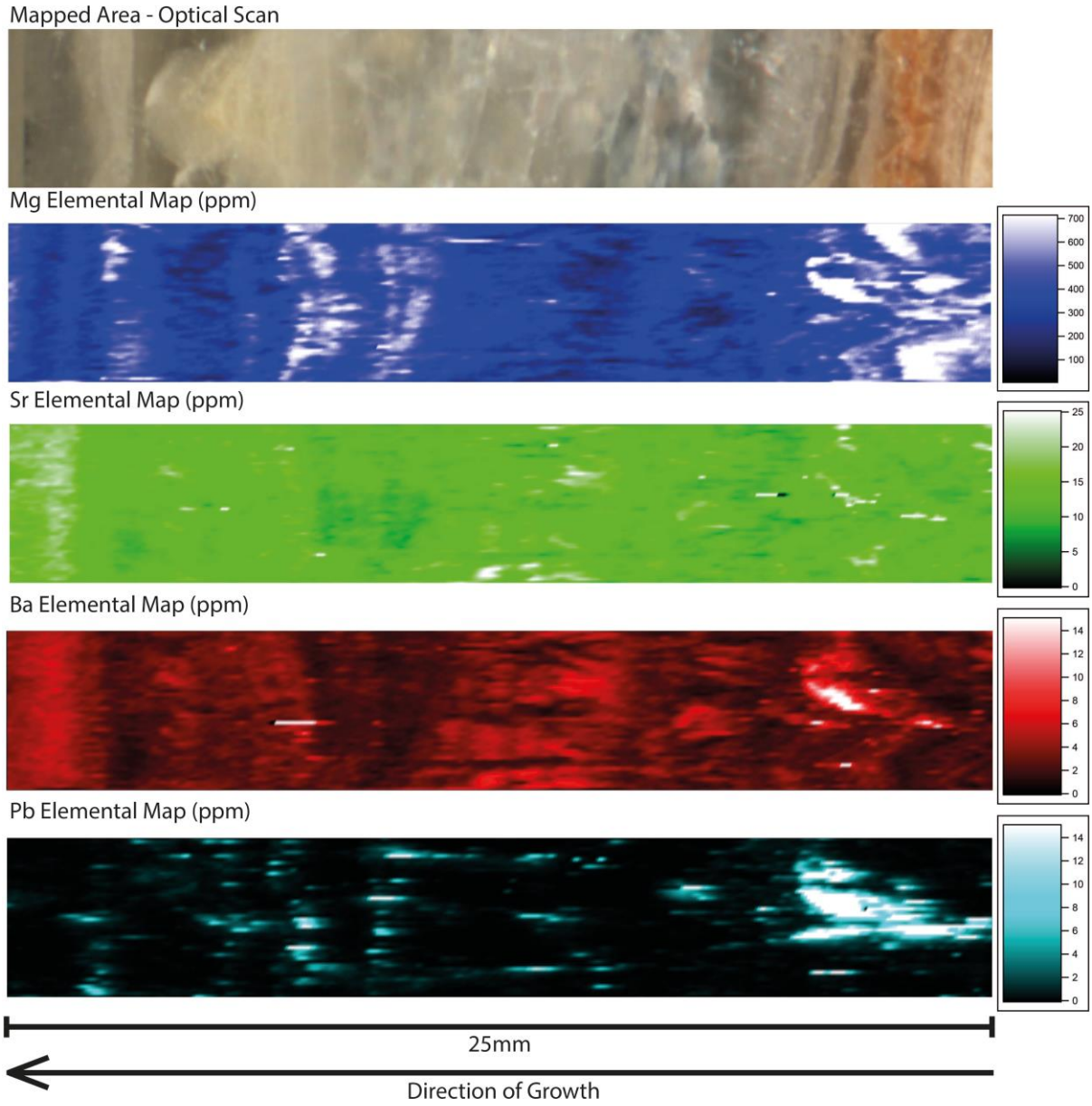

Figure 3: Elemental map of magnesium, strontium, barium and lead concentrations in the right hand mapped area of Figure 2. Concentrations show strong lateral consistency along growth layers. Optical scan image shown for comparison.

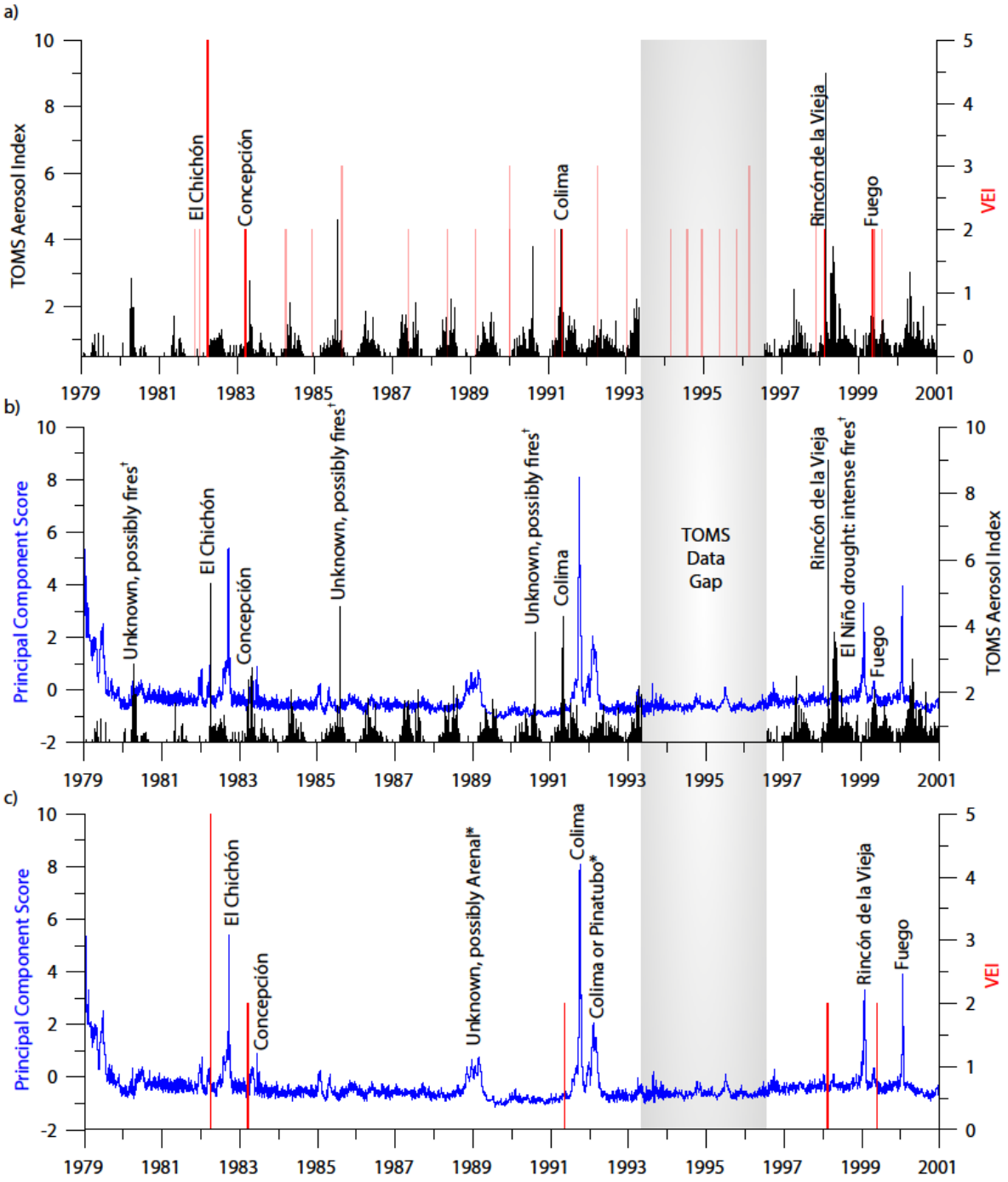

Figure 4: Linking remote sensing derived records of volcanic ash clouds to variations in ATM-7 trace element geochemistry. a) Demonstrating synchronicity of Central American volcanic eruptions of VEI 2 or greater (red) with spikes in TOMS aerosol index above the ATM cave site (black). This identifies

volcanic eruptions with ash clouds which reach the cave site. b) Comparing labelled spikes in TOMS Aerosol Index (black) with PC1 scores over time (blue). c) Volcanic eruptions previously identified as resulting in elevated aerosol levels above the cave plotted against PC1 scores over time. A spike in PC1 follows each of these eruptions within one year. †Elevated Aerosol index levels in these years, which have no corresponding volcanic eruption, due to a higher prevalence of large wildfires due to droughts in El Nino years. *Uncertain records of eruptions; discussed in text.

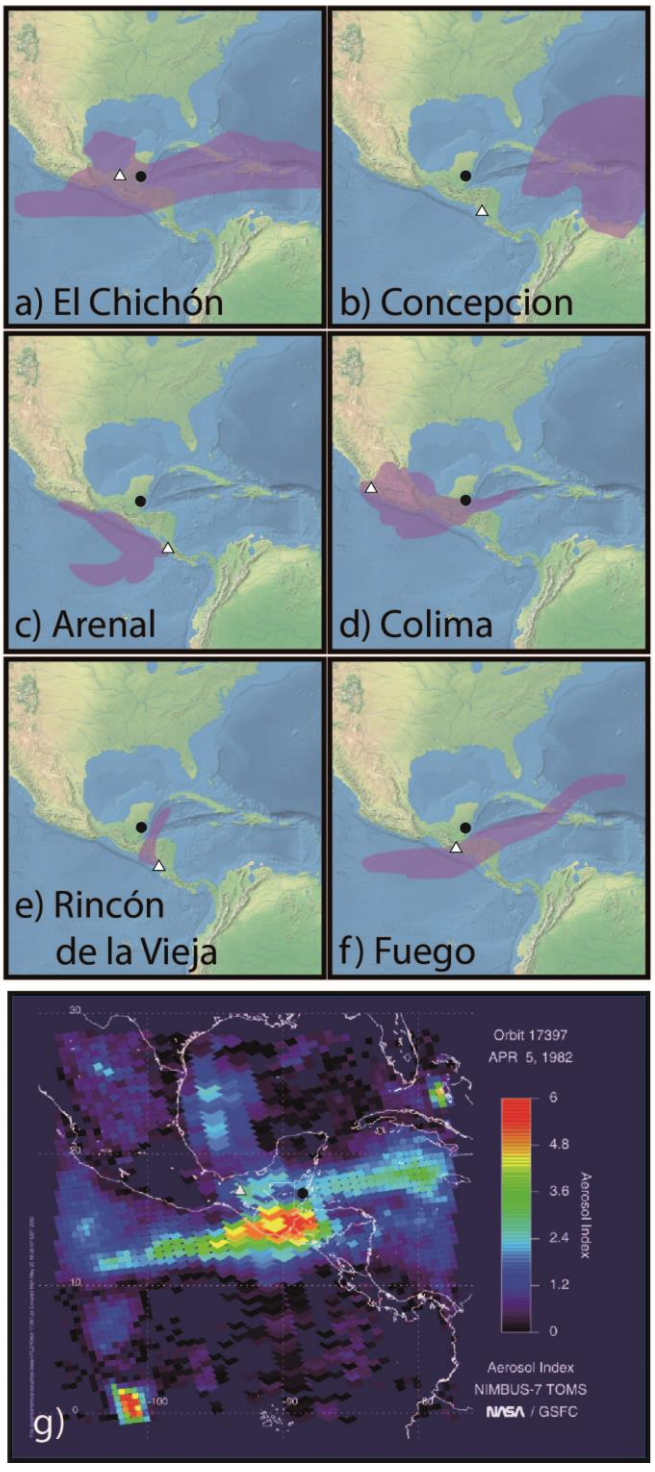

Figure 5: HYSPLIT modelling of ash dispersion 48 hours after eruptions of (a) El Chichón, (b) Concepcion, (c) Arenal, (d) Colima, (e) Rincon de la Vieja, and (f) Fuego. (g) TOMS aerosol index image of El Chichón ash cloud on April 5th 1982 taken approximately one day after the climactic eruption. The triangles mark erupting volcano position, the black circles denote the position of ATM. (a-f) Results of HYSPLIT modelling on the READY system. (g) Courtesy of the NASA TOMS Volcanic Image Archive.

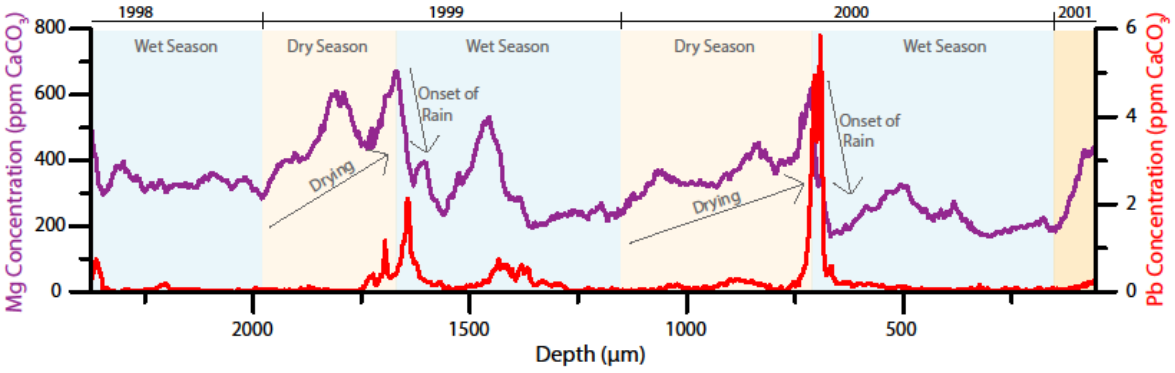

547
548

549 Figure 6: Magnesium concentrations (purple) plotted against lead concentrations (red). Seasonality
550 is inferred from fluctuations in magnesium concentrations, assuming abrupt decreases in Mg

indicate the onset of the wet season and that the initiation of steadily increasing values marks the more gradual onset of the dry season. Lead concentration spikes occur at the start of the wet season, coincident with PC1 spikes, and are interpreted as representing flushing of volcanogenic compounds accumulated in the soil over the previous dry season.

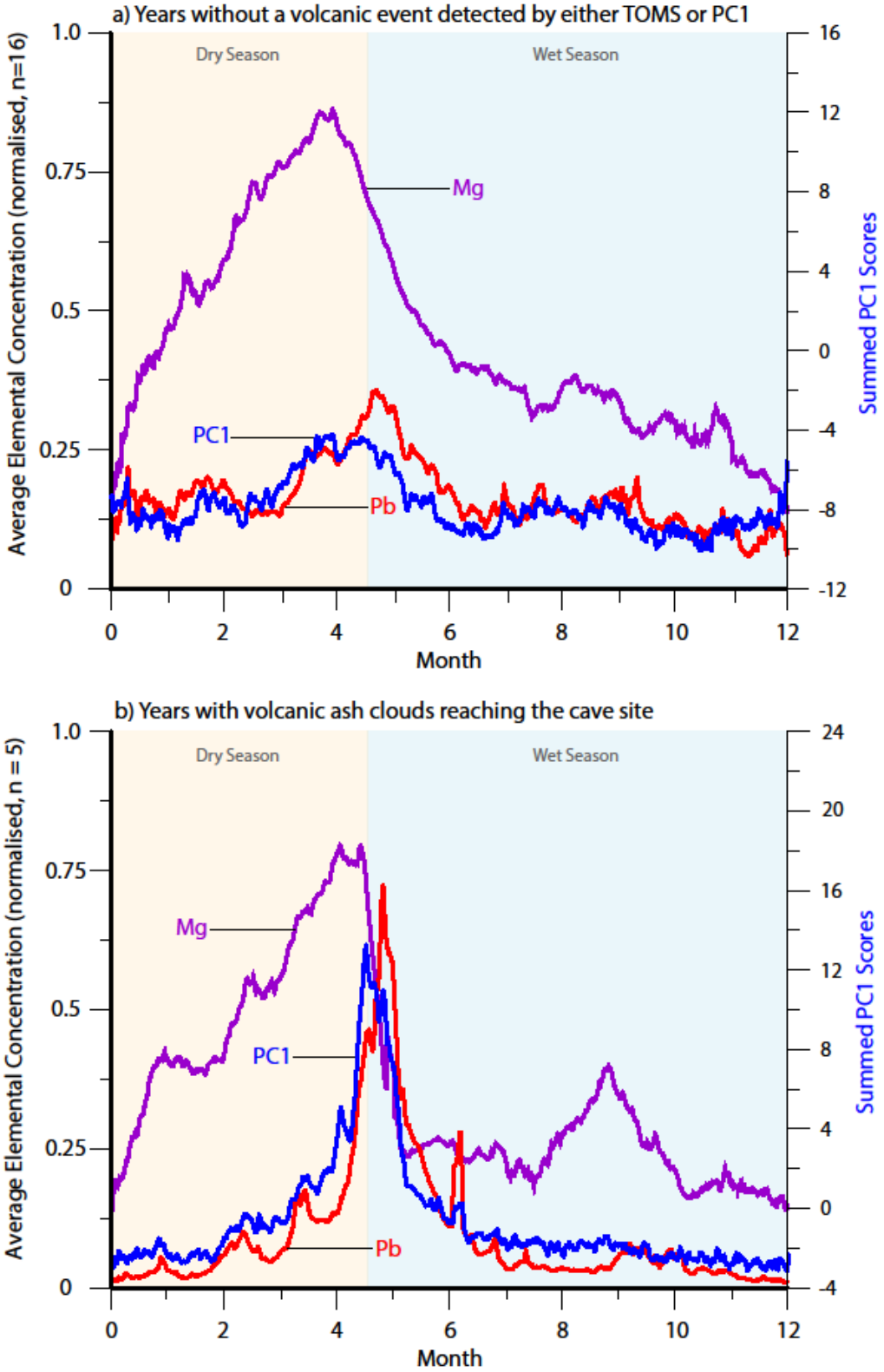
a) Years without a volcanic event detected by either TOMS or PC1
Dry Season
Wet Season
Mg
PC1
Pb
Average Elemental Concentration (normalised, n=16)
Summed PC1 Scores
Month
b) Years with volcanic ash clouds reaching the cave site
Dry Season
Wet Season
Mg
PC1
Pb
Average Elemental Concentration (normalised, n = 5)
Summed PC1 Scores
Month

Figure 7: a) Average patterns of variation during the sixteen years (out of twenty-one total) without an identified eruption affecting the cave site. Magnesium concentrations (purple) are used to infer seasonality. b) Average patterns of variation during the five years with detectable volcanic ash influence. Spikes in lead (red) and PC1 (blue) occur at the onset of the wet season. Elemental concentrations for each year are normalised such that the maximum concentration in the year is equal to one. PC1 scores in each plot are the summed values over the plotted years.

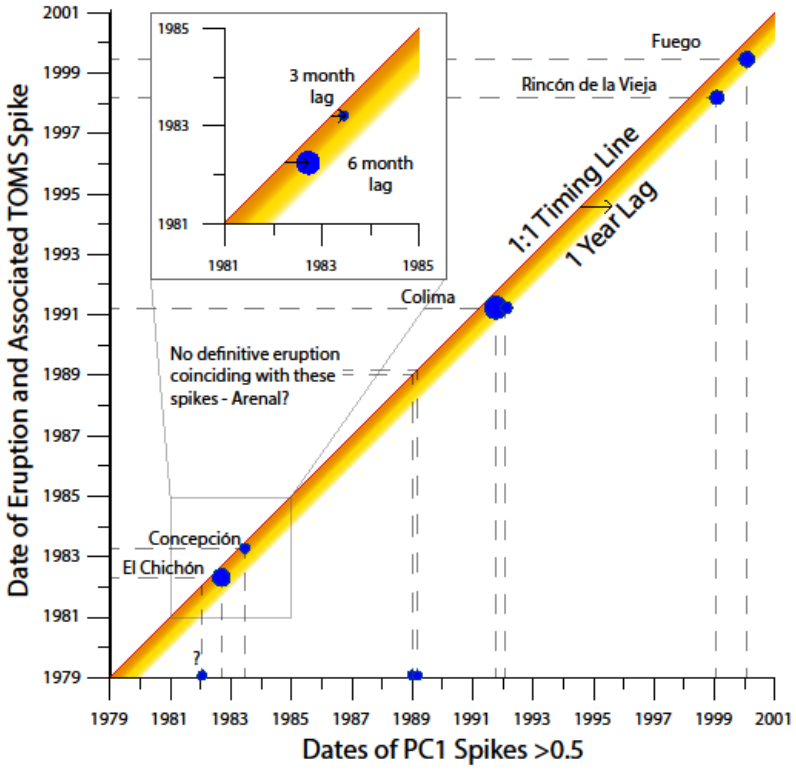
Date of Eruption and Associated TOMS Spike
Dates of PC1 Spikes >0.5
1:1 Timing Line
1 Year Lag
3 month lag
6 month lag
Fuego
Rincón de la Vieja
Colima
Concepción
El Chichón
?
No definitive eruption coinciding with these spikes - Arenal?

Figure 8: Comparison of PC1 spike timings to known eruptions affecting the cave site. Size of markers corresponds to magnitude of PC1 spike. A one-to-one concordance line marks the position where spikes would occur if they were synchronous with the eruptions. All PC1 spikes occur to the right of this line, within up to one year, as expected. Diameter of blue circles is proportional to magnitude of PC1 spike. Markers on x-axis denote PC1 spikes with no definitive corresponding eruption. Insert: length of lag times for El Chichón and Concepción eruptions.

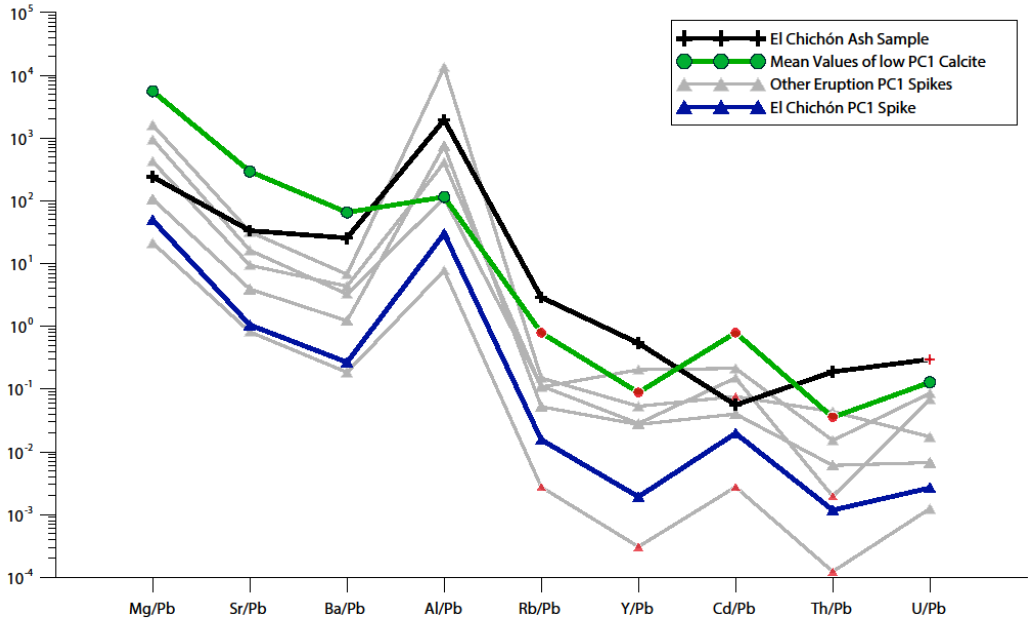

Figure 9: Comparison of geochemistry of stalagmite regions containing ash-derived material compared to mean values of calcite containing no ash signal. Also plotted are the results of ICP-MS analysis of an El Chichón ash sample. All elements ratioed to lead to eliminate the effect of varying amounts of ash-derived material within the speleothem. Symbols in red are values where the concentration of the element analysed are below the detection limits; these are plotted at detection limit values for comparison only whilst the actual values will be lower.

	PC1	Max (ppm)	Median (ppm)	Mean (ppm)	StdDev (ppm)	%RSD
Mg	0.108	1137.22	317.45	348.16	162.04	46.54
Sr	0.070	58.12	12.25	13.13	4.22	32.16
Ba	0.217	109.06	2.68	3.60	5.09	141.84
Al	0.236	13655.19	2.84	138.75	730.31	526.33
Si	0.207	31554.61	1475.52	1526.03	1774.48	116.28
P	0.240	37413.33	12.52	181.91	1496.98	822.93
V	0.238	23.69	0.08	0.26	1.20	459.88
Mn	0.230	58.74	0.65	1.06	3.11	292.25
Fe	0.234	676.20	227.67	230.42	23.93	10.38
Cu	0.243	149.63	1.01	1.95	6.49	332.51
Zn	0.242	466.39	0.37	4.10	21.87	534.15
Rb	0.242	30.40	0.01	0.17	1.35	802.08
Y	0.227	7.44	0.00	0.08	0.54	666.68
Zr	0.244	23.09	0.02	0.17	1.04	603.27
Cd	0.231	5.39	0.00	0.04	0.24	570.04
La	0.233	9.25	0.00	0.08	0.57	681.99
Ce	0.242	12.30	0.00	0.09	0.73	787.31
Pb	0.225	36.48	0.06	0.65	2.41	368.40
Th	0.232	1.95	0.00	0.01	0.10	802.77
U	0.239	2.23	0.01	0.02	0.09	425.74

Table 1: Table of principal component coefficients for Principal Component 1. Also shown are descriptive statistics for the entire dataset population.